Scripta Materialia 272 (2026) 117055

Contents lists available at ScienceDirect

Scripta Materialia

journal homepage: www.journals.elsevier.com/scripta-materialia

Hydrogen plasma-induced blistering on aluminum: morphology, growth, and interfacial energetics

Tong Li, Xiaohan Dai, Jingxuan Su, Degang Xie *

Center for Advancing Materials Performance from the Nanoscale (CAMP-Nano), State Key Laboratory for Mechanical Behaviour of Materials, Xi'an Jiaotong University, Xi'an 710049, PR China

ARTICLE INFO

Keywords:
Aluminum
Hydrogen
Blister
Plasma

ABSTRACT

Hydrogen blistering presents critical reliability concerns in space, nuclear, and semiconductor applications. While prior studies focused on the blister initiation mechanism of nanoscale samples under electron-induced plasma, yet whether similar blistering behavior and mechanism also occur under conventional plasma conditions on bulk materials remain elusive. Here, we show that hydrogen plasma induces extensive blistering on bulk aluminum surface. Atomic force microscopy reveals self-similar blister growth with a nearly constant aspect ratio, consistent with Föppl–von Kármán theory, enabling quantitative extraction of the adhesion energy ($\Gamma \approx 4.83$ J/m^2). We identify two coalescence-driven growth modes—lateral contact- and vertical pile-up-coalescences, and observe blister boundaries with straight segments aligned with crystallographic directions. These features suggest that subsurface nanocavities bounded by low-index facets locally pin the oxide cap. Our findings provide new insights into hydrogen-induced blistering and film delamination and highlight the role of substrate crystallography in shaping interfacial failure.

Main

In hydrogen-containing environments—such as hydrogen plasma [1–3], acidic solutions [4–6], water, and water vapor [7,8]—hydrogen can ingress and accumulate at near-surface defects, particularly at the interface between protective layers and substrates. This segregation can lead to hydrogen blistering, manifested as surface bulging and interface detachment. Hydrogen blistering poses critical challenges in space [1,9], nuclear [10,11], and semiconductor industries [12–14]. In space applications, solar wind composed predominantly of high-energy protons can induce blistering, leading to the degradation of optical components and structural surfaces [9]. In fusion reactors, hydrogen plasma circulating within the Tokamak interacts with plasma-facing materials, leading to blister or bubble formation, mechanical degradation, and protective layer spallation [10,11,15]. In semiconductor fabrication, processes such as atomic layer deposition (ALD) [16,17] may involve hydrogen as a carrier or byproduct, and the residual or environmental hydrogen can cause film blistering, leading to device failure [8,17,18]. Understanding the formation and evolution of hydrogen blisters (also referred to as hydrogen-induced blisters), particularly in plasma environments, is therefore essential for both mitigation strategies and materials design.

Over the past few decades, numerous models have been proposed to describe the nucleation and growth of hydrogen blisters [19–23]. The hydrogen-facilitated vacancy-clustering theory suggests that vacancy clusters—stabilized and enlarged by hydrogen trapping—serve as nucleation sites for blisters [19,20,24]. While this mechanism accounts for intragranular blister formation, it remains unclear whether it also dominates the interfacial blisters, since alternative pathways may be operative and competitive. Our previous studies using in situ environmental transmission electron microscope have elucidated the initiation mechanism of hydrogen blisters at oxide/metal (MO/M) interfaces [21,25]. It has been demonstrated that interfacial hydrogen weakens MO–M bonding [26,27], enabling surface diffusion of metal atoms and the formation of nanoscale cavities via Wulff reconstruction—favorable sites for blister nucleation. Similar cavities have been observed in Al_2O_3/Si systems, which is considered to be caused by Si diffusion [28], suggesting a potentially universal mechanism [28,29]. However, these insights were primarily obtained from nanoscale samples under electron-beam-induced hydrogen plasma in an environmental TEM [21,25], and focus largely on the nucleation stage, leaving the subsequent growth processes—and the resulting diversity in blister

* Corresponding author.
E-mail address: dg_xie@xjtu.edu.cn (D. Xie).

https://doi.org/10.1016/j.scriptamat.2025.117055
Received 24 July 2025; Received in revised form 26 September 2025; Accepted 14 October 2025
Available online 21 October 2025
1359-6462/© 2025 Acta Materialia Inc. Published by Elsevier Inc. All rights are reserved, including those for text and data mining, AI training, and similar technologies.

morphology—poorly understood. In this study, we conducted hydrogen plasma treatment on bulk aluminum samples with commercial purity, characterized and analyzed the morphology of blisters and the underlying substrates, aimed to investigate and the growth mechanism.

Hydrogen plasma experiments were conducted using a custom-built plasma generator (Fig. 1a), comprising a 13.56 MHz radio frequency power supply (maximum output: 600 W), a plasma chamber with upper and lower electrodes inside, and a gas supply system. The system can maintain a stable hydrogen plasma discharge at low pressure (< 200 Pa), emitting a characteristic pink glow (Fig. 1b). In our experiments, high-purity aluminum plates (99.999 %, 10 × 10 mm; Fig. 1c) were cut from a magnetron sputtering target produced by melting and casting. The plates were mechanically polished with 2500-grit sandpaper, followed by electrochemical polishing in a solution of 70 wt.% $HClO_4$ and ethanol (1:9 vol%) at –10 ± 5 °C for ~25 min. Surface quality was examined via scanning electron microscopy (SEM) to ensure smoothness and the absence of scratches, showing no signs of scratches or pollution at the surface (Fig. 1c). The prepared samples were then individually placed on the lower electrode for hydrogen charging. The grain orientations were obtained using electron backscatter diffraction (EBSD) (Fig. 1d) and the average grain diameter was 123.8 μm (Fig. 1e).

The well-polished aluminum plates were then placed into the plasma generator for hydrogen plasma exposure treatment at 15 W in 200 Pa H_2 for 10 min. The plasma treatment was conducted at room temperature without external heating. Because ion impingement inevitably induces some heating, we chose a relatively low plasma power of 15 W to minimize the temperature rise. Immediately after plasma treatment, the sample temperature, measured by an infrared thermometer, remained below 50 °C. Higher plasma powers would induce greater heating, potentially altering the microstructure, accelerating hydrogen diffusion, and intensifying ion bombardment, thereby increasing the likelihood of surface atom sputtering. The chosen plasma power and exposure time were optimized to yield a moderate blister density/size—sufficient for reliable characterization. After plasma treatment, the initially smooth aluminum surface developed pronounced roughness, marked by numerous circular black features (Fig. 2a) with their sizes following a power law distribution (Fig. 2b). Based solely on the SEM image, it remained unclear whether these circular features were hydrogen blisters, as the characteristic surface bulging was not easily discernible. To clarify their nature, we conducted atomic force microscopy (AFM) to characterize the three-dimensional surface morphology. The AFM was carried out on a scanning probe microscope (SPM-9700HT) in dynamic mode with scan rate = 1 Hz and resonant frequency = 200 kHz. AFM topography before hydrogen plasma exposure (Fig. 2c) shows a relatively smooth surface, whereas after hydrogen plasma exposure (Fig. 2d), the surface is populated with semi-spherical protrusions that coincide with circular features, confirming them as hydrogen blisters on bulk, planar aluminum. Accordingly, the surface roughness (Sq) increases from 1.7 nm to 19.8 nm during the hydrogen charging. Occasionally, ruptured blisters were observed (Fig. 2e), exposing hollow interiors capped by a thin film. These observations indicate that the blisters originate from delamination of the native oxide layer, driven by hydrogen accumulation at the oxide–metal interface. Rupture likely occurs when continued expansion reduces the oxide film thickness below its fracture threshold. This mechanism aligns with previous reports [21,29] of interfacial blistering induced by hydrogen.

The sample surface was densely populated with oxide film blisters of varying sizes, indicative of different growth stages. This diversity allowed us to investigate the blister growth mechanism by reconstructing the morphological evolution from size-resolved features. Specifically, we analyzed the radius (r) and maximum height (h) of individual blisters within the AFM-scanned region to determine the evolution of their aspect ratio (h/r) with size. The blisters ranged in diameter from several tens to ~500 nm. As shown in Fig. 2f, across this size range, nearly all blisters exhibit a spherical-cap morphology with similar aspect ratio of $h/r \approx 0.38$, with only ~11 % variation. The nearly invariant aspect ratio, independent of blister size, indicates that blister growth proceeds in a self-similar manner as shown in the inset of Fig. 2f.

Similar behavior has been reported in other film–substrate systems, including 2D materials [30–33], where the aspect ratio h/r serves as a critical dimensionless parameter governed by the energetical balance between elastic deformation and interfacial adhesion, independent of the trapped material [32]. In this context, the observed self-similar growth suggests an energetically balanced regime, in which the bending energy of the oxide film and the energy required for delamination propagation remain in equilibrium, leading to isotropic expansion and a constant aspect ratio [30].

The observed blistering phenomenon can be described by Föppl–von Kármán (FvK) theory, which, in the large-deflection regime of thin film ($t \ll r$ and $h \gg t$, t is film thickness), links the interfacial adhesion energy Γ to the film's elastic and geometric parameters. In our case, $t < 7$ nm [21], far smaller than both the blister r and h (tens to thousands of nanometers), fulfilling the required criteria and justifying use of the FvK framework to estimate Γ [34,35]. The FvK equations [36–38] express the relationship between blister aspect ratio and adhesion energy as:

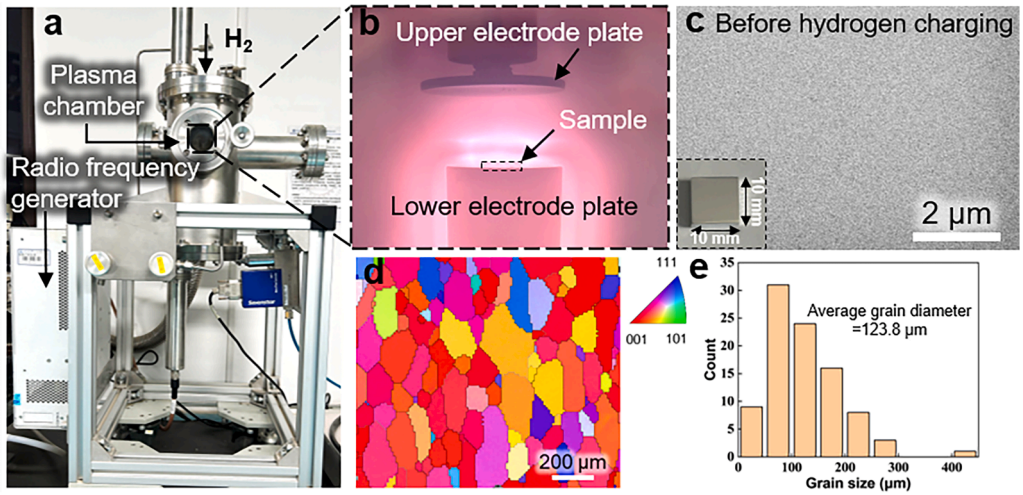


Fig. 1. Experimental set up for hydrogen plasma charging. (a) Home-built hydrogen plasma generator used for hydrogen charging. (b) The hydrogen plasma generated between two electrodes, where sample is placed on the lower electrode. (c) SEM image of the sample surface before hydrogen charging. The insert is a well-polished aluminum sample. (d) The EBSD map of the tested sample. (e) The grain size data obtained from (d).

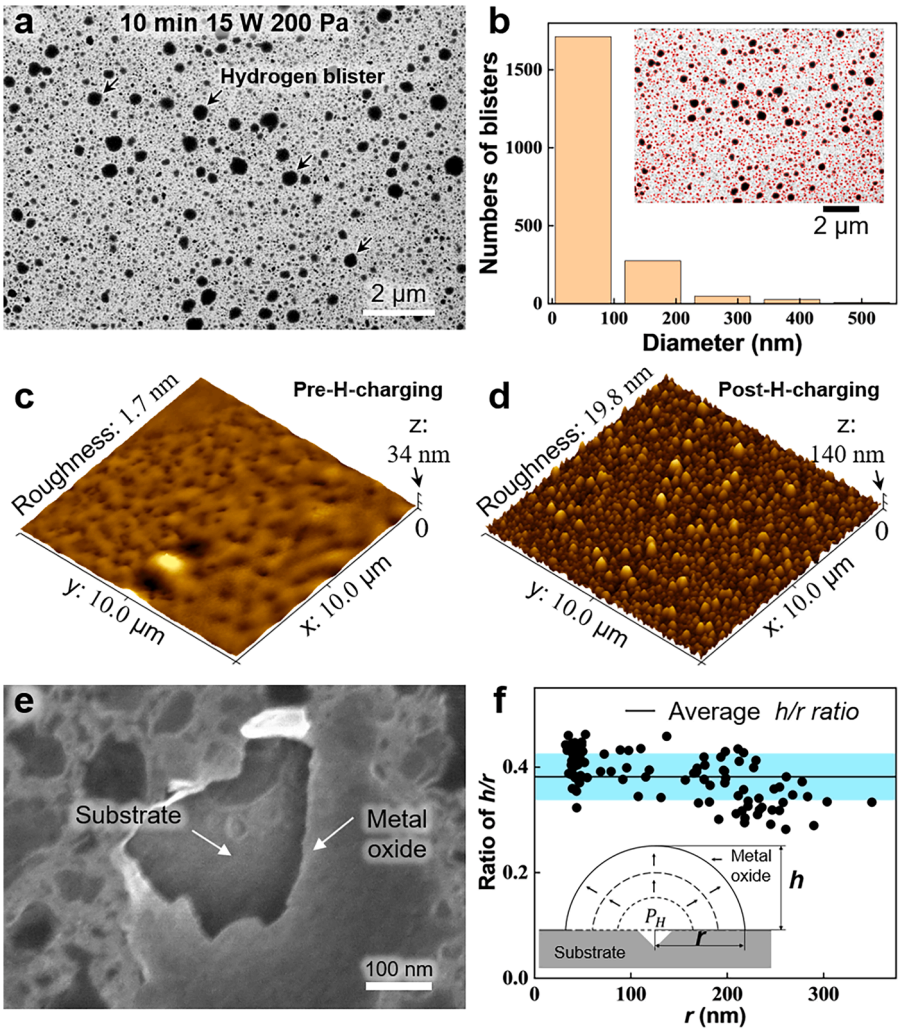


Fig. 2. Hydrogen blister morphology on the aluminum and self-similar growth of blisters. (a) SEM image of the sample surface after hydrogen charging. (b) Size distribution of blisters identified in (a); the inset highlights the detected blister profiles (red circles). (c, d) AFM images of the surface topography before and after hydrogen charging, respectively. (e) SEM image of a fractured blister, revealing its internal structure. (f) Distribution of the aspect ratio (h/r), where h and r denote blister height and radius, respectively; the inset provides a schematic of the self-similar blister growth process.

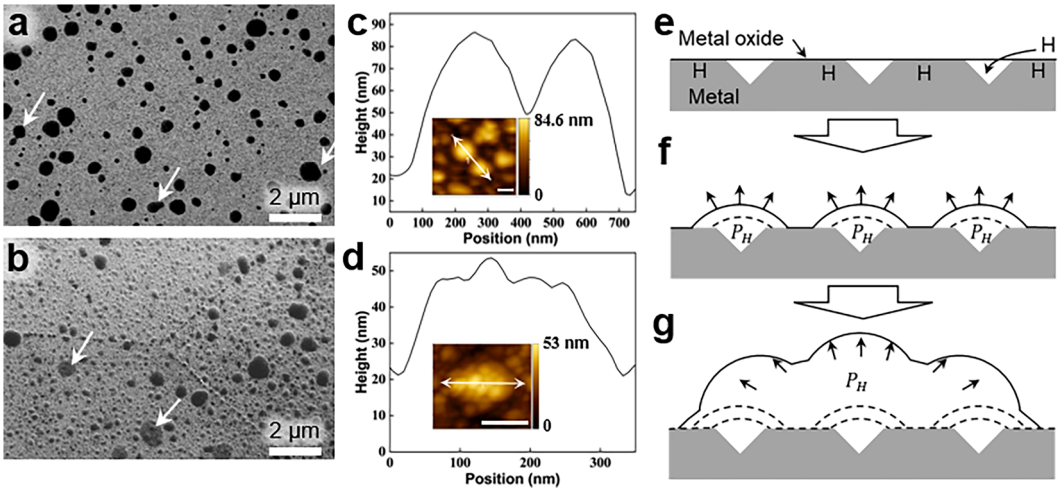


Fig. 3. Growth of hydrogen blisters via contact- and pile-up-coalescence. (a, b) SEM images showing blisters (white arrows) formed by lateral coalescence and vertical pile-up-coalescence, respectively. (c, d) One-dimensional tomographic scans of contact- and pile-up-coalesced blisters; insets show corresponding AFM images (scale bars: 200 nm). White arrows indicate the scanning lines. (e–g) Schematics illustrating the vertical pile-up coalescence process of blisters.

$$\frac{h}{r} = \left(\phi \frac{\Gamma}{E_{2D}}\right)^{\frac{1}{4}} \quad (1)$$

where ϕ is a dimensionless coefficient dependent on the Poisson's ratio ν of the membrane, E_{2D} is the Young's modulus of the 2D material. Under the strong shear limit [37], $\phi = 24(1\text{-}\nu)/5(7\text{-}\nu)$ where $\nu = 0.24$ for Al_2O_3 film [39], we obtain $\phi = 0.54$. By inserting the Young's modulus of the Al_2O_3 film (125 GPa [40–42]) and the measured blister dimensions into the model, the adhesion energy was estimated as $\Gamma = 4.83$ J/m^2. This value lies between the adhesion energies of $Al/Al_2O_{3(O)}$ (10.095 J/m^2) and $Al/Al_2O_{3(Al)}$ (1.078 J/m^2) obtained through first-principles calculations [43], and is therefore physically reasonable. These results establish a quantitative framework for extracting membrane–substrate adhesion energies directly from blister geometry.

In addition to the typical blisters exhibiting smooth spherical-cap morphologies, we also observed untypical blister shapes, suggesting the presence of alternative growth mechanisms. As shown in Fig. 3a, some larger blisters each have a neck in the middle part (white arrows), possibly resulting from a merging process between two closely spaced blisters. AFM topography and 1-dimensional tomographic scan across these blisters (Fig. 3c) confirm the lateral contact-coalescence, revealing the neck-like bridge has a saddle shape and the oxide film there has been lifted due to relaxation after blister coalescence.

In some cases, large blisters were observed with multiple smaller blisters protruding from their caps (Fig. 3b, white arrows). These smaller blisters did not appear to be in direct contact with each other. Rather, they seem to have nucleated and grown on the surface of a preexisting large blister. AFM topography and the 1-dimensional tomographic scan (Fig. 3d) revealed a large plateau on the center of the blister cap, featuring multiple peaks—indicative of superimposed bulging events. We propose that when several small, closely spaced blisters form in proximity, the interfacial regions between them—severely weakened by hydrogen segregation—may progressively detach, thereby enabling the connection of gas pockets across neighboring blisters (Fig. 3e–g). Once this occurs, the detached region expands as a whole, while the small blisters on the cap remain largely unchanged and appear as secondary protrusions. Because the growth of an individual blister is constrained by the internal hydrogen pressure and the mechanical properties of the surface film, its growth rate is inherently limited. In contrast, the blister coalescence mechanisms observed—both lateral coalescence and vertical pile-up-coalescence—provide a far more efficient pathway for expanding the interfacial detachment area, and thus may represent the dominant processes driving large-scale delamination and film spallation.

Together, these observations reveal two distinct coalescence-driven blister growth modes: the first one is lateral coalescence of two neighboring blisters, forming a single expanded structure with a bridged neck; the other one is vertical pile-up-coalescence, where closely packed small blisters within a confined area result in collective interfacial delamination and formation of a large blister, with remnant micro-blisters retained on its surface.

Now we have studied the initiation and growth of hydrogen blisters on the flat surface of a bulk aluminum sample. We are still curious that under the oxide cap, whether similar nano-cavitation process [21] occurs to result in a dimpled surface on the metal substrate. For this purpose, we conducted a mechanical exfoliation of blisters to expose the substrate under the oxide film, as shown in Fig. 4a. Carbon adhesive tape was used to peel off the oxide layer of the blister cap. As shown in Fig. 4b-c, the caps of large blisters were readily removed. Overall, 27 % of the blisters ruptured, with nearly all large blisters (98 % with diameter > 800 nm) failing. However, since the exfoliation experiments were conducted in air, re-oxidation will happen immediately after peeling off the oxide cap. The following SEM characterization only revealed a rough substrate surface, consisting of islands of nano oxides with sizes of a few tens of nanometers, as shown in Fig. 4d-f. These results indicate that the substrate cannot be a perfect smooth one. However, this evidence is still not enough to conclude that nano-cavitation occurs at the initiation stage of the blisters.

Although most blisters appear circular at first glance, closer inspection reveals that many boundaries contain straight segments, and in some cases, the entire blister adopts a polygonal shape, as shown in Fig. 5a-b. The straight edges, represented by red and white lines, appear to be parallel to certain intersection lines (illustration in Fig. 5a-b) between the surface and low index crystallographic planes of the metal substrate. From the AFM results, straight edges or boundaries can also be identified, as shown in Fig. 5c.

The observed deviation from circularity indicates local anisotropic influences during blister growth. In isotropic systems, blisters are expected to adopt spherical-cap geometries with circular boundaries, as predicted by thermodynamic theory [35,44]. In our case, the relevant parameters—the gas pressure, the mechanical response of the amorphous oxide film, and the adhesion at the oxide–metal interface—are all nominally isotropic [32,33]. Under such conditions, the spherical cap

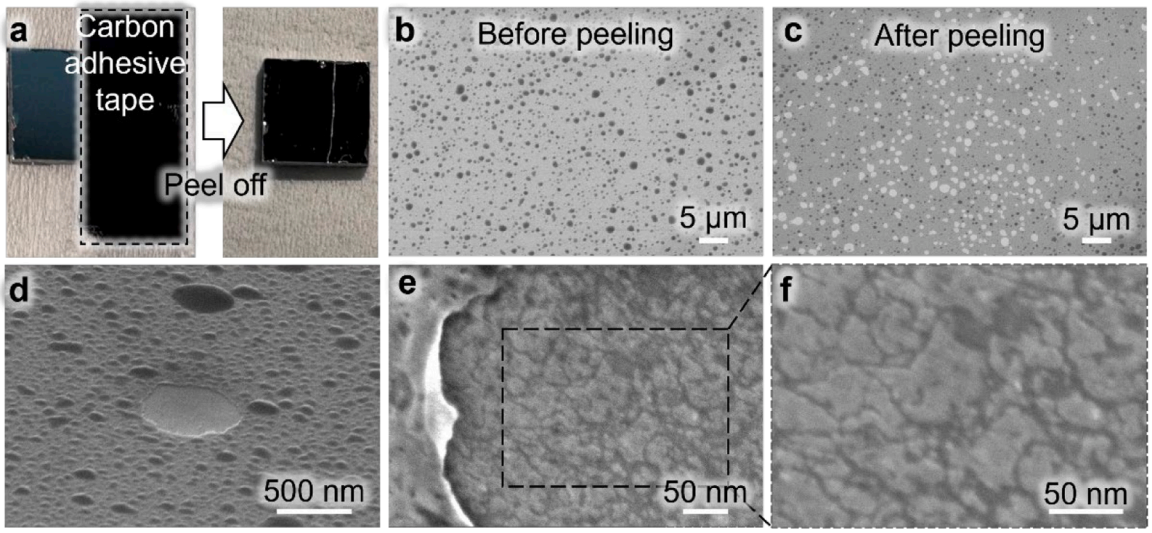


Fig. 4. Mechanical peeling of blistered aluminum to reveal underlying substrate morphology. (a) Optical images of the aluminum sample before and after peeling with carbon adhesive tape. (b-c) SEM images of the sample surface before and after peeling, respectively. (d–f) SEM images at increasing magnifications showing the morphology of the substrate exposed beneath the peeled blisters.

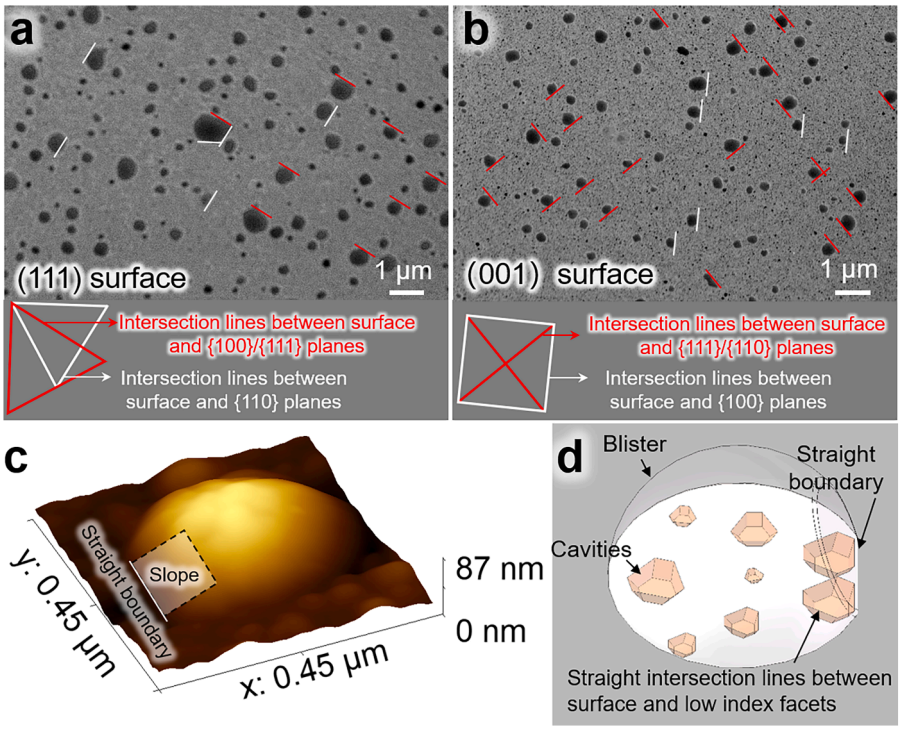


Fig. 5. Blisters with straight boundary segments and their analysis. (a, b) SEM images showing two representative sets of straight blister boundaries (marked by red and white lines) that appear parallel on the (111) and (001) surfaces, respectively. The accompanying illustrations depict the intersections between these crystal surfaces and the low-index planes {110}, {100}, and {111} of the metal substrate. (c) AFM image showing a blister with a straight boundary; the white line marks the straight edge, and the dashed square highlights the associated local planar region of the blister cap. (d) Schematic illustration suggesting that straight blister boundaries may result from pinning by straight edges of substrate cavities intersecting the surface.

should represent the energy-minimizing configuration. However, the underlying aluminum substrate is crystalline and exhibits anisotropy. Our previous studies indicate that nanocavities bounded by low-index crystallographic facets—such as {100}, {110}, and {111}, though not limited to these—can form beneath the blister caps [21]. These faceted cavities intersect the surface, producing straight edges at the substrate surface in the blister cap, as shown in Fig. 5d. These edges likely act as pinning sites, locally impeding the radial expansion of the oxide cap and facilitating the formation of straight segments within an otherwise circular boundary. Statistical analysis reveals that many of these straight segments are mutually parallel and roughly aligned with the projected intersection lines of low-index planes with the sample surface, as indicated by the same-colored straight lines in Fig. 5a-b, consistent with their origin from subsurface nanocavities. Minor deviations from the ideal crystallographic directions may result from factors such as interfacial defects, local surface roughness, or interactions with nearby blisters.

Taken together, these observations indicate that while blister growth is primarily governed by isotropic thermodynamic forces, the substrate crystallography introduces localized anisotropic perturbations. We interpret the presence of straight edges and polygonal boundaries as secondary effects superimposed on a fundamentally isotropic growth mode. Although these crystallographic features modify the cap boundary locally (Fig. 5c, d), they do not alter the dominant spherical-cap morphology.

In summary, this study elucidates the morphology and growth mechanisms of hydrogen blisters formed on bulk aluminum surfaces under hydrogen plasma exposure. We demonstrate that blistering originates from hydrogen accumulation at the oxide–metal interface, driving delamination of the native oxide film and leading to surface bulging. AFM analysis reveals a self-similar growth mode characterized by a nearly invariant aspect ratio, consistent with an energetic balance between elastic deformation and interfacial adhesion. By applying the Föppl–von Kármán framework, we quantify the adhesion energy at the interface, offering a useful metric for evaluating film–substrate adhesion. Beyond the canonical spherical-cap morphology, we identify two distinct coalescence-driven growth modes and uncover the emergence of faceted, polygonal blister boundaries. These non-ideal geometries are attributed to crystallographically defined nanocavities that locally pin the oxide cap, introducing anisotropic perturbations into an otherwise isotropic expansion. Together, these findings provide mechanistic insights into both the nucleation and growth of hydrogen blisters in metal–oxide systems and underscore the critical role of substrate crystallography in shaping interfacial failure modes.

CRediT authorship contribution statement

Tong Li: Writing – original draft, Methodology, Investigation, Formal analysis, Data curation. **Xiaohan Dai:** Writing – review & editing, Formal analysis. **Jingxuan Su:** Investigation, Writing – review & editing. **Degang Xie:** Writing – review & editing, Supervision, Methodology, Funding acquisition, Formal analysis, Conceptualization.

Declaration of competing interest

The authors declare that they have no known competing financial interests or personal relationships that could have appeared to influence the work reported in this paper.

Acknowledgments

This work was supported by the National Natural Science Foundation of China (52371122) and Shaanxi Province Foundation for Distinguished Young Scholars (2024JC-JCQN-47). We thank Hang Guo at Instrument Analysis Center of Xi'an Jiaotong University for their assistance with AFM analysis.

References

[1] M. Sznajder, U. Geppert, M.R. Dudek, Hydrogen blistering under extreme radiation conditions, Npj Mater. Degrad. 2 (2018) 3.
[2] D. Shefer, A. Nikipelov, M. Van De Kerkhof, Z. Marvi, V. Banine, J. Beckers, The impact of hydrogen plasma on the structure and morphology of tin and lead micrometer sized particles, J. Phys. Appl. Phys. 56 (2023) 085204.
[3] D. Wan, Y. Deng, A. Barnoush, Hydrogen embrittlement effect observed by in-situ hydrogen plasma charging on a ferritic alloy, Scr. Mater. 151 (2018) 24–27.
[4] P. Rozenak, Hemispherical bubbles growth on electrochemically charged aluminum with hydrogen, Int. J. Hydrog. Energy 32 (2007) 2816–2823.
[5] V. Singh, R. Singh, K.S. Arora, D.K. Mahajan, Hydrogen induced blister cracking and mechanical failure in X65 pipeline steels, Int. J. Hydrog. Energy 44 (2019) 22039–22049.
[6] S. Zhang, Q. Zhao, J. Liu, F. Huang, Y. Huang, X. Li, Understanding the effect of niobium on hydrogen-induced blistering in pipeline steel: a combined experimental and theoretical study, Corros. Sci. 159 (2019) 108142.
[7] J.L. Smialek, Moisture-induced TBC spallation on turbine blade samples, Surf. Coat. Technol. 206 (2011) 1577–1585.
[8] G.M. Scamans, A.S. Rehal, Electron metallography of the aluminium-water vapour reaction and its relevance to stress-corrosion susceptibility, J. Mater. Sci. 14 (1979) 2459–2470.
[9] M. Sznajder, P. Seefeldt, T. Spröwitz, T. Renger, J.H. Kang, R. Bryant, W. Wilkie, Solar sail propulsion limitations due to hydrogen blistering, Adv. Space Res. 67 (2021) 2655–2668.
[10] K. Ouaras, M. Redolfi, D. Vrel, C. Quirós, G. Lombardi, X. Bonnin, K. Hassouni, Tungsten blister formation kinetic as a function of fluence, ion energy and grain orientation dependence under hydrogen plasma environment, J. Fusion Energy 37 (2018) 144–153.
[11] M.Y. Ye, H. Kanehara, S. Fukuta, N. Ohno, S. Takamura, Blister formation on tungsten surface under low energy and high flux hydrogen plasma irradiation in NAGDIS-I, J. Nucl. Mater. 313 (316) (2003) 72–76.
[12] A. Agarwal, T.E. Haynes, V.C. Venezia, O.W. Holland, D.J. Eaglesham, Efficient production of silicon-on-insulator films by co-implantation of He^+ with H^+, Appl. Phys. Lett. 72 (1998) 1086–1088.
[13] G. Cerofolini, Hydrogen and helium bubbles in silicon, Mater. Sci. Eng. R Rep. 27 (2000) 1–52.
[14] O. Beldarrain, M. Duch, M. Zabala, J.M. Rafí, M.B. González, F. Campabadal, Blistering of atomic layer deposition Al_2O_3 layers grown on silicon and its effect on metal–insulator–semiconductor structures, J. Vac. Sci. Technol. Vac. Surf. Films 31 (2013) 01A128.
[15] A. Makarochkin, E. Yahel, G. Makov, Blister growth model in proton-irradiated metals - application to tungsten irradiated by MeV protons, J. Nucl. Mater. 564 (2022) 153712.
[16] C. Bohórquez, J.L. Vazquez, L.E. López, J.A. Jurado, D. Domínguez, O.E. Contreras, H.J. Tiznado, Exploring Al_2O_3 blister evolution through cathodoluminescence and attenuated total reflectance infrared analyses, J. Vac. Sci. Technol. A 42 (2023) 012403.
[17] S. Zhao, G. Yuan, D. Zhang, P. Xu, G. Li, W. Han, Formation and elimination mechanism of thermal blistering in Al_2O_3/Si system, J. Mater. Sci. 56 (2021) 17478–17489.
[18] P. Saint-Cast, D. Kania, R. Heller, S. Kuehnhold, M. Hofmann, J. Rentsch, R. Preu, High-temperature stability of c-Si surface passivation by thick PECVD Al_2O_3 with and without hydrogenated capping layers, Appl. Surf. Sci. 258 (2012) 8371–8376.
[19] J.B. Condon, T. Schober, Hydrogen bubbles in metals, J. Nucl. Mater. 207 (1993) 1–24.
[20] X.C. Ren, Q.J. Zhou, G.B. Shan, W.Y. Chu, J.X. Li, Y.J. Su, L.J. Qiao, A nucleation mechanism of hydrogen blister in metals and alloys, Metall. Mater. Trans. A 39 (2008) 87–97.
[21] D.-G. Xie, Z.-J. Wang, J. Sun, J. Li, E. Ma, Z.-W. Shan, In situ study of the initiation of hydrogen bubbles at the aluminium metal/oxide interface, Nat. Mater. 14 (2015) 899–903.
[22] M.C. Tiegel, M.L. Martin, A.K. Lehmberg, M. Deutges, C. Borchers, R. Kirchheim, Crack and blister initiation and growth in purified iron due to hydrogen loading, Acta Mater. 115 (2016) 24–34.
[23] J. Hou, X.-S. Kong, X. Wu, J. Song, C.S. Liu, Predictive model of hydrogen trapping and bubbling in nanovoids in bcc metals, Nat. Mater. 18 (2019) 833–839.
[24] Y. Fukai, Superabundant vacancies formed in metal-hydrogen alloys, Phys. Scr. T103 (2003) 11.
[25] M. Li, D.-G. Xie, E. Ma, J. Li, X.-X. Zhang, Z.-W. Shan, Effect of hydrogen on the integrity of aluminium–oxide interface at elevated temperatures, Nat. Commun. 8 (2017) 14564.
[26] R.A. Oriani, P.H. Josephic, Equilibrium aspects of hydrogen-induced cracking of steels, Acta Metall. 22 (1974) 1065–1074.
[27] M.S. Daw, M.I. Baskes, Semiempirical, quantum mechanical calculation of hydrogen embrittlement in metals, Phys. Rev. Lett. 50 (1983) 1285–1288.
[28] M. Broas, H. Jiang, A. Graff, T. Sajavaara, V. Vuorinen, M. Paulasto-Kröckel, Blistering mechanisms of atomic-layer-deposited AlN and Al_2O_3 films, Appl. Phys. Lett. 111 (2017) 141606.
[29] M. Zamanzade, C. Müller, J.R. Velayarce, C. Motz, Susceptibility of different crystal orientations and grain boundaries of polycrystalline Ni to hydrogen blister formation, Int. J. Hydrog. Energy 44 (2019) 7706–7714.
[30] W. Wang, X. Ma, Z. Dai, S. Zhang, Y. Hou, G. Wang, Q. Li, Z. Zhang, Y. Wei, L. Liu, Mechanical behavior of blisters spontaneously formed by multilayer 2D materials, Adv. Mater. Interfaces 9 (2022) 2101939.
[31] Y. Rao, E. Kim, Z. Dai, J. He, Y. Li, N. Lu, Size-dependent shape characteristics of 2D crystal blisters, J. Mech. Phys. Solids 175 (2023) 105286.
[32] E. Khestanova, F. Guinea, L. Fumagalli, A.K. Geim, I.V. Grigorieva, Universal shape and pressure inside bubbles appearing in van der Waals heterostructures, Nat. Commun. 7 (2016) 12587.
[33] W. Wang, S. Chen, J. Cao, X. Wei, Z. Dai, Round and pleated blisters: interface delamination in thin film deposition, Int. J. Smart Nano Mater. 16 (2025) 343–358.
[34] E.H. Mansfield, The Bending and Stretching of Plates, 2nd ed., Cambridge University Press, Cambridge, England, 1989.
[35] J. Cao, Z. Dai, C. Yu, W. Wang, X. Wei, Y. Wei, Fracture mechanics of 2D crystal blisters with irregular geometry, Adv. Funct. Mater. (2025) e09438.
[36] M. Pandey, G. Wang, G. Singh, R. Ahuja, R. Kumar, Instabilities in the blistering of two-dimensional materials, 2D Mater. 12 (2025) 022008.
[37] D.A. Sanchez, Z. Dai, P. Wang, A. Cantu-Chavez, C.J. Brennan, R. Huang, N. Lu, Mechanics of spontaneously formed nanoblisters trapped by transferred 2D crystals, Proc. Natl. Acad. Sci. 115 (2018) 7884–7889.
[38] K. Yue, W. Gao, R. Huang, K.M. Liechti, Analytical methods for the mechanics of graphene bubbles, J. Appl. Phys. 112 (2012) 083512.
[39] D.C. Miller, R.R. Foster, S.-H. Jen, J.A. Bertrand, S.J. Cunningham, A.S. Morris, Y.-C. Lee, S.M. George, M.L. Dunn, Thermo-mechanical properties of alumina films created using the atomic layer deposition technique, Sens. Actuators Phys. 164 (2010) 58–67.
[40] G. Alcalá, P. Skeldon, G.E. Thompson, A.B. Mann, H. Habazaki, K. Shimizu, Mechanical properties of amorphous anodic alumina and tantala films using nanoindentation, Nanotechnology 13 (2002) 451–455.
[41] D. Mercier, V. Mandrillon, G. Parry, M. Verdier, R. Estevez, Y. Bréchet, T. Maindron, Investigation of the fracture of very thin amorphous alumina film during spherical nanoindentation, Thin Solid Films 638 (2017) 34–47.
[42] Z. Xia, L. Riester, W.A. Curtin, H. Li, B.W. Sheldon, J. Liang, B. Chang, J.M. Xu, Direct observation of toughening mechanisms in carbon nanotube ceramic matrix composites, Acta Mater. 52 (2004) 931–944.
[43] W. Zhang, J.R. Smith, Nonstoichiometric interfaces and Al_2O_3 adhesion with Al and Ag, Phys. Rev. Lett. 85 (2000) 3225–3228.
[44] A. Ishii, Influence of elastic anisotropy on the shapes of ellipsoidal blisters and stress field around the blisters in solid materials, AIP Adv. 13 (2023) 125024.